The effects of exhaust plume and nozzle length on transonic axisymmetric base flows using Tomographic PIV

Brust, Steve; van Gent, Paul; Schrijer, Ferdinand; van Oudheusden, Bas

The effects of exhaust plume and nozzle length on transonic axisymmetric base flows using Tomographic PIV

S.G. Brust, P.L. van Gent, F.F.J. Schrijer, B.W. van Oudheusden. Delft University of Technology

An experimental campaign has been conducted to investigate the effect of nozzle length and exhaust plume presence on the flow topology aft of a transonic launch vehicle. To this end, Tomographic PIV is used to acquire mean-velocity data in the base flow region bounded by the main body and the nozzle of the axisymmetric model. The region of interest features a strong, separated shear layer and its reattachment point which divides the freestream and a low-pressure recirculation region behind the base. To study these effects in a structured manner a wind tunnel model is produced which allows for a variable, effective nozzle length and which features a "cold-plume" exhaust jet. It is found that the length of the nozzle and the presence of the plume have a significant effect on the overall flow topology and velocity fluctuations.

Model specifics are described in further detail in section 1.1. The PIV setup, which is used to capture all necessary data, is described in section 1.2 along with relevant processing in section 1.3. Results are presented in section 2. Lastly, in section 2.1, a momentum based pressure reconstruction is used to analyze the effect on mean-pressure in the field of view.

1 Experimental Arrangements

All experimental results presented herein were gathered at the Transonic/Supersonic TST-27 wind tunnel of the aerodynamics laboratory at the TU Delft. This is a blowdown type windtunnel covering a Mach range from 0.5 to 4.2 with a maximum run time of approximately 300 seconds. The test section has a width of 280mm and a height of 270mm. Pressure is supplied to the settling chamber via a 300 m^3 vessel pressurized to a maximum of 40 bar. The diameter based Reynolds number, $Re_D = 1.5e6$ while testing at a set $M = 0.7$. The freestream flow variables are rescaled to account for the presence of the model in the test section; said rescaling is based on a steady pressure transducer measurement on the model and upstream of the field of view. This results in a freestream velocity, $V_\infty = 245ms^{-1}$, temperature, $T_\infty = 257K$, and pressure, $p_\infty = 1.01$ at $M_\infty = 0.75$.

1.1 The model

The model, seen in Figure 1 is a modification of the FESTIP model [3] for which new nozzle and backplate pieces are designed and produced. Depres et. al. [1] identified three cases which will yield a shear layer impingement location on the nozzle, near the nozzle exit, or in the exhaust plume; in the present experiment this is facilitated by two additional collars that slide over the nozzle and attach to the backplate thus reducing the nozzle length from 90 mm to either 60 mm or 30 mm. The three tested cases are defined as $L/D = 1.8$, $L/D = 1.2$, and $L/D = 0.6$, respectively. Additionally, an underexpanded exhaust plume is introduced which exits the model at $M_{jet} = 4.0$ with a nozzle pressure ratio, $NPR = 100$.
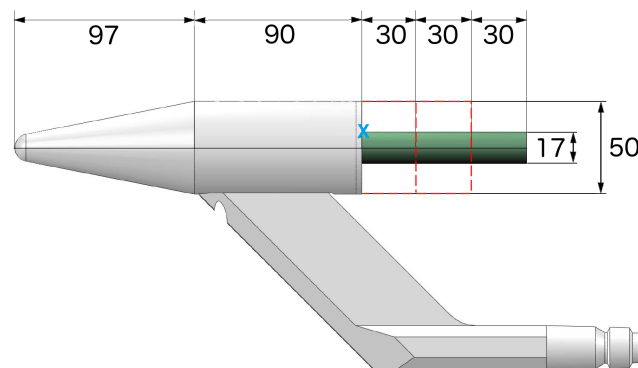

Figure 1: Dimensions of the variable nozzle length, cold-plume equipped test model; the blue 'x' indicates the reference frame origin.

1.2 PIV setup

To ensure a statistically converged flow field, 500 image pairs are captured using the following equipment (All results presented herein use 250 of those images). The PIV setup incorporates 5 Imperx B1610M Bobcat 2 Mpix CCD cameras fitted with 72mm Tamron lenses set to f#5.6; this yields a focal depth of approximately 9 mm. Cameras are arranged in a cross-like setup with a system aperture angle, $\beta = 45°$ to provide an optimal reconstruction quality factor (Scarano [4]). Illumination of the field of view is provided by a 400 mJ per pulse Nd:YAG Spectra Physics laser. The dimensions of the field of view are approximately 90 by 70 by 8 mm. DEHS seeding particles are used with a nominal diameter of 1 μm and are introduced in the settling chamber upstream of the test section; A PIVTEC DEHS Atomizer seeder, set to 1 bar above total pressure, is used to atomize the particles and seed the flow. The DEHS particles have a relaxation time, τ_p of 2 μs (Ragni et. al. [2]).

1.3 PIV processing

PIV preprocessing is done using LaVision DaVis 8.3.1; the following steps are performed to mitigate reflections and increase signal-to-noise ratios leading to an improved volumetric reconstruction. Firstly, all pixels which display the model are disabled as these are the greatest source of reflections. Additionally, an algorithmic mask is applied in cases which include strong reflections coming from the exhaust plume. All individual images are then normalized using a local average with a radius of 6 pixels after which a sliding average is subtracted with a 6 pixel scale length. Volumetric reconstruction is done by way of a FastMART approach in which a 50% valid voxel requirement, per window, is enforced. Cross-correlation of the volumes is done in five passes with an elliptical window size that gradually decreases from 96 to 32 voxels with a constant 75% overlap; this results in a vector pitch of 0.34 mm. Lastly, vector postprocessing is conducted using universal outlier detection and said outliers are replaced with a linear interpolation of adjacent data points.

2 Results

Presented in Figure 2 are the mean streamwise velocity components normalized with the freestream velocity for the cases without an exhaust plume. Herein, the approximate shear layer reattachment location is visible; well within the exhaust area for $L/D = 0.6$, near the nozzle exit for $L/D = 1.2$, and well upstream of the nozzle exit for $L/D = 1.8$ as was predicted by Depres et. al. [1]. Figure 3 shows the same configurations with jet and it is found that this does not have a noticeable effect on the reattachment location of the shear layer.
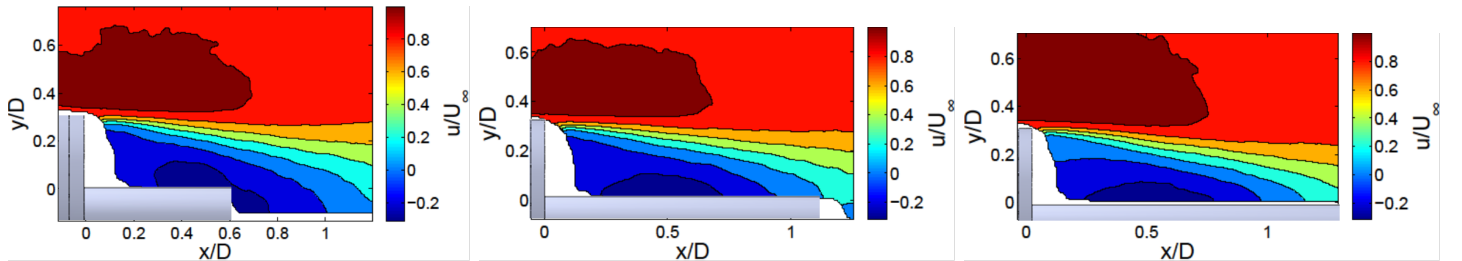

Figure 2: Visible shear layer reattachment locations for cases without an exhaust plume and nozzle lengths, $L/D = 0.6$, 1.2, and 1.8 (From left to right)

It is found, however, that maximum backflow velocities in the recirculation region are changed by the presence of an exhaust plume as seen in Figure 3. In the two longer nozzle length cases it is observed that the maximum backflow velocity decreases slightly with the presence of an exhaust plume and the point of highest velocity moves forward by approximately 3 mm. The opposite is observed for the shortest case, $L/D = 0.6$ because the presence of the jet causes a significantly stronger backflow region increasing the maximum observed backflow velocity from 0.31 U_∞ to 0.33 U_∞ while doing little to change the location of maximum backflow.
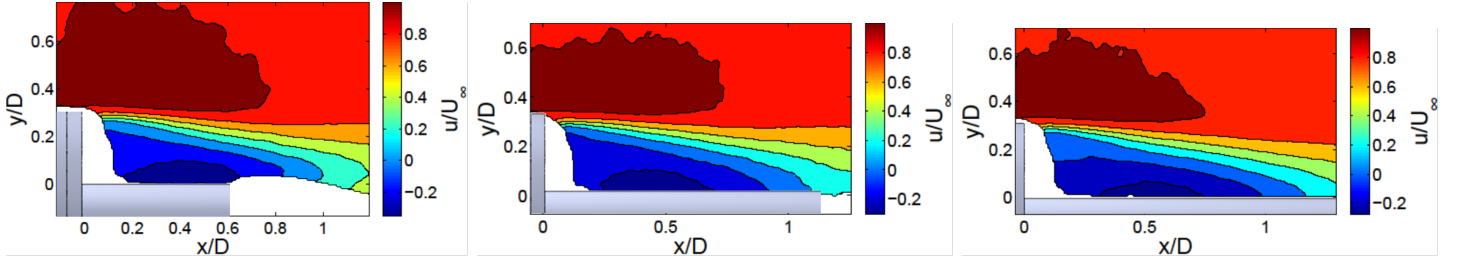
Figure 3: Visible shear layer reattachment locations for cases with an exhaust plume and nozzle lengths, $L/D = 0.6$, 1.2, and 1.8 (From left to right)

The normalized radial RMS components are shown in Figure 4 for the exhaust-jet cases. It can be seen that for the $L/D = 1.2$ case that there is a higher RMS value in the recirculation region; this could potentially be attributed to a higher degree of turbulent mixing taking place due to the ingestion of exhaust gases into the recirculation region.
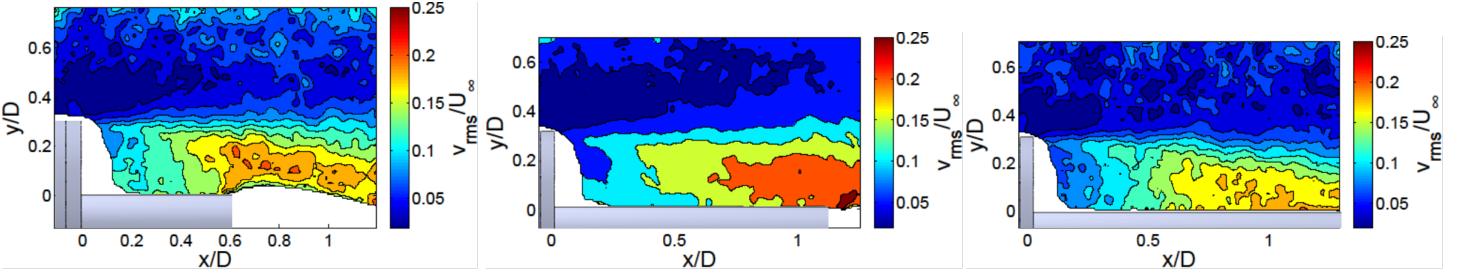

Figure 4: Radial RMS component normalized with freestream velocity, U_∞ for cases with an exhaust plume and nozzle lengths, $L/D = 0.6$, 1.2, and 1.8 (From left to right)

The turbulent mixing in the shear layer can be quantified by the Reynolds shear stress. The values for the three cases with jet are shown in Figure 5. Although the overall ensemble size is too small to have converged statistics, it can be seen that the mid-length configuration ($L/D = 1.2$) produces the highest Reynolds stresses in the vicinity of flow reattachment.
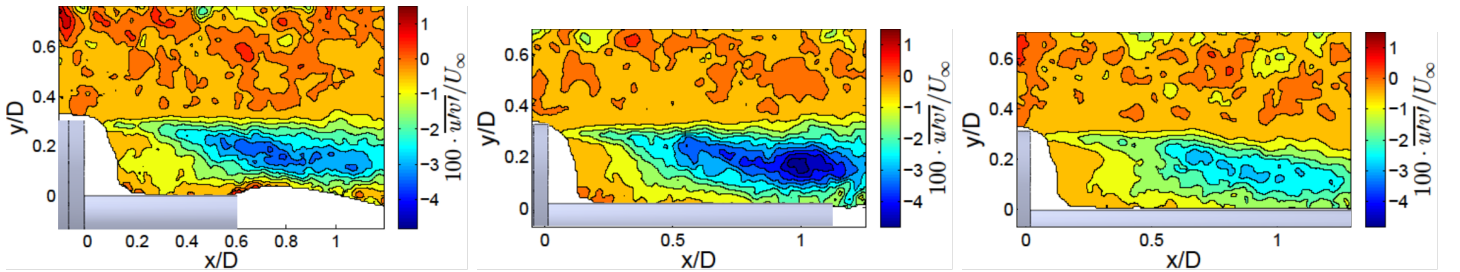

Figure 5: Reynolds stress plotted as $100 \cdot \overline{u'v'}/U_\infty$ for cases with an exhaust plume and nozzle lengths, $L/D = 0.6$, 1.2, and 1.8 (From left to right)

2.1   Mean-pressure reconstruction

The pressure field reconstruction makes use of the momentum equation in order to calculate the pressure gradient using the experimentally measured velocity data. By assuming inviscid and adiabatic flow, the effects of compressibility are accounted for by allowing a reformulation of the momentum equation in which density is an independent variable as outlined by van Oudheusden [3]. The assumptions of inviscid and adiabatic flow are considered valid due to the high Reynolds number of the flow and the absence of heat transfer in the region of interest, respectively.

The results of the pressure reconstruction are visible in Figure 6 and Table 1. The difference seen in pressure coefficient values between cases with and without a jet is in line with what is described by Depres et. al. [1] as the "jet-suction" effect. It can be seen that the presence of an exhaust jet reduces the mean-pressure aft of the base by a consistent difference.
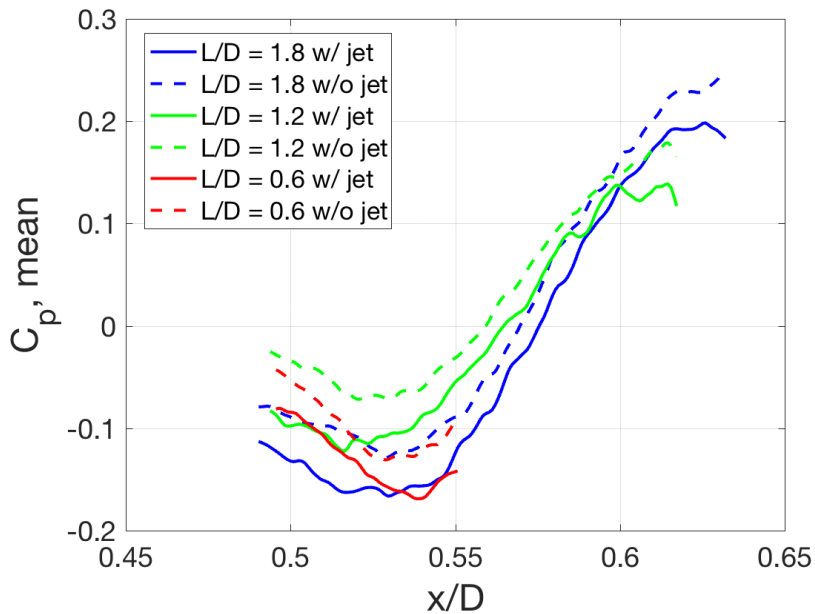
Figure 6: Mean-pressure coefficient comparison between all cases

L/D	0.6	1.2	1.8
min. C_p w/o jet	-0.13	-0.07	-0.12
min. C_p w/ jet	-0.17	-0.12	-00.16
ΔC_p	0.033	0.036	0.36

Table 1: A comparison of recorded minimum C_p values

3   Conclusion

Presented herein are the findings for an experimental investigation of the effect of nozzle length and exhaust plume on the mean flow topology aft of a transonic launch vehicle. There are noticeable changes to the flow topology that can partially be attributed to the differences in configuration that were tested. The most turbulent case is that which features the mid-length nozzle ($L/D = 1.2$) and the presence of an exhaust jet; this is due to the fact that recirculation region and exhaust plume are in contact with one another, causing higher fluctuation values than seen in other cases. Conversely, the case which keeps these two significant flow features properly separated sees the lowest velocity fluctuations.

References

[1] Deprés, D., P. Reijasse, and J. P. Dussauge. "Analysis of unsteadiness in afterbody transonic flows." AIAA journal 42.12 (2004): 2541-2550.

[2] Ragni, D., et al. "Particle tracer response across shocks measured by PIV." Experiments in fluids 50.1 (2011): 53-64.

[3] Van Oudheusden, B. W. "PIV-based pressure measurement." Measurement Science and Technology 24.3 (2013): 032001.

[4] Scarano, F. "Tomographic PIV: principles and practice." Measurement Science and Technology 24.1 (2012): 012001.